

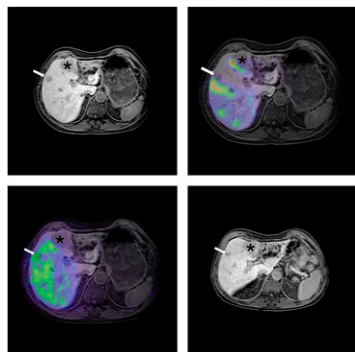
**Hybrid SLN biopsy guidance:** van den Berg and colleagues provide an update and overview of technological innovations that can improve surgical guidance during sentinel lymph node biopsy procedures. . . . . *Page 493*

**PET, RT, and head and neck cancer:** Menda and Buatti look at current evidence supporting the predictive utility of early PET imaging during radiotherapy in patients with head and neck cancer. . . . . *Page 497*

**Functional PET in uterine tumors:** Zhao and colleagues investigate information about sex hormone receptors and indices of tumor proliferation provided by <sup>18</sup>F-FES and <sup>18</sup>F-FDG PET in patients with mesenchymal uterine tumors. . . . *Page 499*

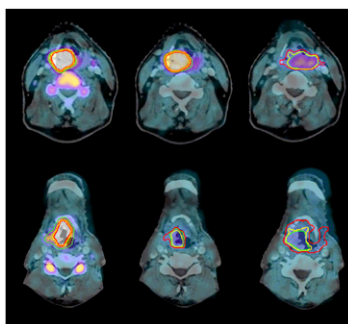
**<sup>18</sup>F-FDG PET/CT in T/NK cell lymphomas:** Li et al. assess the value of interim and posttherapy PET/CT as predictors of progression-free and overall survival in T-cell and natural killer lymphomas. . . . . *Page 507*

**<sup>99m</sup>Tc-MAA uptake in CRC liver lesions:** Ulrich and colleagues research the predictive value of pretherapy intratumoral <sup>99m</sup>Tc-MAA uptake on perfusion scintigraphy in patients with colorectal liver metastases scheduled for <sup>90</sup>Y-microsphere radioembolization. . . . . *Page 516*

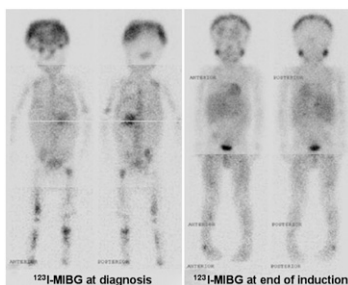


**Brown fat O<sub>2</sub> consumption:** Muzik and colleagues determine to what extent brown adipose tissue thermogenesis is activated during cold stress in an effort to elucidate relationships between <sup>18</sup>F-FDG tracer uptake on PET and brown fat oxidative metabolism. . . . . *Page 523*

**<sup>18</sup>F-FLT PET and early therapy response:** Hoeben and colleagues study the use of sequential <sup>18</sup>F-FLT PET to monitor early response to radiation or chemotherapy for head and neck cancer. . . *Page 532*



**Prognostic impact of mIBG scoring:** Yanik and colleagues from the Children's Oncology Group look at the predictive capabilities of metaiodobenzylguanidine imaging in patients with stage 4 neuroblastoma at various time points in diagnosis and treatment. . . . . *Page 541*



**Artificial intelligence SPECT:** Arsanjani and colleagues report on efforts to improve

the diagnostic accuracy of automatic myocardial perfusion SPECT interpretation analysis for prediction of coronary artery disease by integrating quantitative perfusion and functional variables using a computer machine learning method. . . . . *Page 549*

**CZT MPI SPECT and LV function:** Cochet and colleagues evaluate myocardial perfusion imaging using cadmium-zinc-telluride SPECT cameras to measure left ventricular global and regional function and also assess absolute wall motion and thickness measurements with cardiac MR as a reference. . . . . *Page 556*

**Sex differences in extraaortic <sup>18</sup>F-FDG:** Kaneko and colleagues describe differences in extraaortic arterial <sup>18</sup>F-FDG accumulation in asymptomatic men and women to clarify the association between such accumulation and both cardiovascular risk factors and coronary artery stenosis. . . . . *Page 564*

**Software reproducibility of <sup>82</sup>Rb PET MBF:** deKemp and colleagues detail the performance of 3 highly automated software programs commonly used for absolute myocardial blood flow and flow reserve assessment with <sup>82</sup>Rb PET imaging. . . . . *Page 571*

**<sup>99m</sup>Tc(CO)<sub>3</sub>(NTA) and <sup>131</sup>I-OIH:** Taylor and colleagues compare the pharmacokinetics of these tracers in imaging patients with stage 3–4 renal failure and describe the potential of the new <sup>99m</sup>Tc agent for routine clinical measurement of effective renal plasma flow. . . . . *Page 578*

**PET/CT lymphoscintigraphy in oral cancer:** Heuveling and colleagues investigate the clinical feasibility of PET/CT lymphoscintigraphy using <sup>89</sup>Zr-nanocolloidal albumin in patients with early-stage oral cancer. . . . . *Page 585*

**Dynamic bone imaging:** Wong and Piert offer an educational overview of the mech-

anisms of uptake of  $^{99m}\text{Tc}$ -labeled diphosphonates and  $^{18}\text{F}$ -sodium fluoride and discuss and compare the performance of these bone-seeking radiotracers in clinical and research applications. . . **Page 590**

**In vivo  $B_{\text{max}}$  and  $K_d$  of  $^{11}\text{C}$ -GR103545:** Tomasi and colleagues describe the development of this selective  $\kappa$ -opioid receptor PET tracer and the results of a study in rhesus monkeys to estimate in vivo receptor concentration and dissociation equilibrium constant. . . . . **Page 600**

**PET and cardiac hypertrophy:** Zhong and colleagues use a mouse model of transverse aortic constriction to explore the hypothesis that metabolic remodeling with increased  $^{18}\text{F}$ -FDG uptake precedes and triggers severe contractile dysfunction in

pressure-overload left ventricular hypertrophy. . . . . **Page 609**

**Imaging V/Q in a model of COPD:** Jobse and colleagues assess ventilation/perfusion SPECT imaging in mouse studies to determine the ways in which chronic exposure to cigarette smoke affects the lungs, with special reference to early functional changes. . . . . **Page 616**

**Hepatobiliary transport and SPECT:** Neyt and colleagues demonstrate a noninvasive method to visualize and quantify disturbances in hepatic uptake and biliary efflux of  $^{99m}\text{Tc}$ -mebrofenin. . . **Page 624**

**4D CT generation from 4D PET:** Fayad and colleagues present a method for dy-

namic CT image generation from a combination of a reference CT image and deformation matrices obtained from elastic registration of 4D PET images not corrected for attenuation. . . . . **Page 631**

**Optical/nuclear small-animal imaging:** Solomon and colleagues report on a fiber-based fluorescence-mediated tomography system combined with a preclinical SPECT/CT platform and results in proof-of-concept studies in rats. . . . . **Page 639**

**Guidelines for inflammation/infection imaging:** Donohoe and other experts from the SNMMI and the European Association of Nuclear Medicine detail new evidence-based guidelines for performing  $^{18}\text{F}$ -FDG PET or PET/CT in inflammation and infection. . . . . **Page 647**

## ON THE COVER

As can be seen in this patient, SPECT/CT clarifies the anatomic location of the SLNs located outside the extended pelvic lymphadenectomy field (white and pink arrows).

See page 493.

